Integral equations for the interpretation of MT and GDS results

Ulrich Schmucker, Göttingen

1. The linearization of the EM inverse problem

We assume that electromagnetic (EM) response estimates are available for a set of discrete frequencies ω_n, in case of 2D or 3D interpretations also for various field sites at surface locations $\underline{r} = (x, y, 0)$. Cartesian coordinates are used, with *z* positive down. To be found are models of conductivity or resistivity within a modelling domain *A* in the lower half-space. Regardless of their specific nature, the complex-valued estimates will be denoted with $y_n(\underline{r})$ and called henceforth *the datum*, with $\Delta y_n(\underline{r})$ as the stochastic error of its absolute value. Let the model generate the theoretical datum $y_n^{(\mathrm{mod})}(\underline{r})$ for the same frequency and location. Then the difference $\delta y_n(\underline{r}) = y_n(\underline{r}) - y_n^{(\mathrm{mod})}(\underline{r})$ represents the misfit residual for the respective datum and model, with

$$\delta y^2 = <| \delta y_n(\underline{r}) |^2> \tag{1}$$

as mean squared residual, when < > implies an average over all data. Let correspondingly

$$\Delta y^2 = < \Delta y_n(\underline{r})^2 > \tag{2}$$

be the mean squared data error. Then the interpretation will be regarded to be within error limits, when δy and Δy are equal. Data of very uneven quality should be weighted with their reciprocal rms errors Δy_n prior to their interpretation.

A functional F_n shall connect datum and model in $y_n^{(\mathrm{mod})}(\underline{r}) = F_n(x \mid \underline{r},)$, depending on the entire model in *A*,. It can be an algorithm or for example a numerical FD solution. A frequently used interpretation method, based on a Taylor expansion of a starting model, converts the non-linear inverse problem into an approximated linear problem with the aid of derivatives $\partial F_n / \partial x$. Its solution leads to successive model improvements $\delta x(\underline{r}')$ as they follow from the misfit residuals $\delta y_n(\underline{r})$ for the model in the foregoing iteration or the starting model, yielding a better fit to the data. Here we shall adopt a different approach by formulating the forward problem as an integral equation with an integrand which is decomposed into a *known* data kernel $K_n(x \mid \underline{r}, \underline{r}')$ and an *unknown* model parameter $x(\underline{r}')$ at the internal point $\underline{r}'$, in the1D case for example the logarithm of resistivity:

$$y_n(\underline{r}) = \int_A K_m(x \mid \underline{r}, \underline{r}') \cdot x(\underline{r}')\, d\underline{r}' + \delta y_n . \tag{3}$$

The non-linearity of the inverse problem is preserved in the indicated model-dependence of the data kernel. The key point is now to define data and model for a data kernel, which depends only weakly on the model, and that a completely model-independent data kernel can be formulated to begin an iterative process, during which an entirely new model is derived in each iteration rather than stepwise model improvements.

2. The iterative process of modelling and its inherent problems

The process is initiated not with a *preconceived* starting model as it is usually done, but with an approximated starting kernel $K_n^{(0)}(\underline{r},\underline{r}')$ which is model-independent. It replaces in eq. (3) the data kernel $K_n(x\,|\,\underline{r},\underline{r}')$ for the not yet known model $x(\underline{r}')$. Solving then this equation toward the model parameters leads to a *data-derived* starting model $x^{(0)}(\underline{r}')$. It is used to calculate a now model-dependent data kernel $K_n^{(1)}(x^{(0)}\,|\,\underline{r},\underline{r}')$, which may or may not be closer to the data kernel for the final model. Eq. (3) is solved again with this kernel towards a second model $x^{(1)}(\underline{r}')$, and so on. If iterations converge, data kernels and models become more and more consistent with each other, and the process can be terminated, when the change of models and kernels between consecutive iterations is below chosen thresholds..

The advantages are twofold. (i) Because models follow directly from the data and not from misfit residuals, data errors are readily converted into model errors as shown in the next section.. (ii) For the same reason the model resolution can be quantified in terms of a resolution kernel. Due to the limited number of error-bearing data, the obtained model parameters have to be understood in general as spatial mean values $\bar{x}(\underline{r}'_k)$ of the "true" model in some neighbourhood of an internal point $\underline{r}' = \underline{r}'_k$ according to

$$\bar{x}(\underline{r}'_k) = \int_A a(\underline{r}'_k,\underline{r}')\, x(\underline{r}')\, d\underline{r}' \;, \tag{4}$$

with $a(\underline{r}'_k,\underline{r}')$ as resolution kernel for the so-called *target point* $\underline{r}'_k$. The closeness of $a(\underline{r}'_k,\underline{r}')$ to a delta- function for a perfect resolution expresses the achieved degree of resolution at the target point. Measures of resolution are

$$\Delta(\underline{r}'_k) = \int_A [a(\underline{r}'_k,\underline{r}') - \delta(\underline{r}'_k - \underline{r}')]^2\, d\underline{r}' \tag{5a}$$

or, with $J(\underline{r}'_k,\underline{r}')$ as "anti-delta-function, the *Backus-Gilbert spread*

$$\Delta(\underline{r}'_k) = \int_A a(\underline{r}'_k,\underline{r}')^2\, J(\underline{r}'_k,\underline{r}')\, d\underline{r}' \;. \tag{5b}$$

The smaller these measures, the better the model resolution around the target point.

Problems which may arise in the course of the above described iterative process are likewise twofold. Firstly, the iterative process will not converge, when the approximated starting kernel $K_n^{(0)}(\underline{r},\underline{r}')$ is too different from the kernels in the following iterations. In that case iterations should be started with the kernel for a preconceived model which can be thought to be closer to the final model. Secondly, in 2D and 3D interpretations conductivity or resistivity may turn negative. Such non-physical results can be encountered when interpreting error-bearing data which are inconsistent with *any* model, or when the data base is too small for the chosen complexity of the model. In principle negative values can be avoided by increased smoothing of the model by stronger regularisation, but on the expense that the misfit residuals may become too large in comparison to the data errors. Obviously, the second problem does

not exists when the logarithm of conductivity or resistivity serves as model parameter, as it is the case here for 1D interpretations, and which is common practice for interpretations based on incremental improvements of a starting model.

The iterative process has to be interrupted, when one or more model parameters attain a non-physical value, and an intermediate iterative process is conducted in the form of an algorithm described by Lawson & Hanson (1974, Section 23.3). Its purpose is to solve linear problems by least squares under side conditions in the form of inequalities, for example that no discrete model parameter x_m may be smaller than a specified threshold value x_L. After completion the algorithm assigns the model parameters to two classes. The first class contains all parameters with $x_m > x_{lL}$ and $\partial Q / \partial x_m = 0$ as least squares condition, when Q denotes the squared residual norm. Parameters assigned to the second class have values at the lower limit and exclusively positive derivatives $\partial Q / x_m$. Hence, their increase beyond x_L increases Q and thereby leads to a poorer than least squares fit to the data. Consequences for model interpretations will be one of the topics in Section 8..

Kalscheuer & Pedersen (2007) have considered in similar ways modelling errors and the resolution of 2D models, which have been obtained on the basis of derivatives of the functional and successive model improvements, as briefly outlined above. Their conclusions involve the following underlying assumptions. The model response y_n^* for the next to final iteration has to be regarded as error-free, which implies that the data errors are also the errors of the misfit residuals in the last iteration, which lead to the final model. Correspondingly, the next to last model has to be regarded as error-free in order that the errors of the last model improvement as derived now from the data errors represent also the errors for the final model.

3. The four modes of model derivation

For clarity we consider in this section a modelling space which is subdivided into M uniform layers or grid cells with a constant discrete model parameter x_m. Furthermore, the data are now numbered in sequence for frequency *and* field sites. If N_1 is the number of frequencies and N_2 the number of field sites, then the total number of data is $N = N_1 \cdot N_2$. In the notations of eqs (1) and (3) the resulting linear system of N equations for M unknowns is

$$y_n = \sum_{m=1}^{M} K_{nm} x_m + \delta y_n , \tag{6}$$

for n=1,2,…,N and without explicitly expressing the model-dependence of the data kernel. Its general solution in terms of a spatially averaged model parameter for a chosen target layer or cell $m = k$ is

$$\bar{x}_k = \sum_{n=1}^{N} h_{kn} y_n , \tag{7}$$

while the model resolution for this layer or cell is expressed in correspondence to eq. /(4) by

$$\bar{x}_k = \sum_{m=1}^{M} a_{km} x_m \tag{8}$$

with the now discrete resolution coefficients a_{km} .The squared modelling error in terms of the solution coefficients h_{kn} is

$$\Delta\bar{x}_k^2 = \sum_{n=1}^{N} h_{kn}^2 \, \Delta y_n^2 \quad , \tag{9}$$

as it is readily inferred from eq. (7) for statistically independent random data errors Δy_n. We consider now the data kernel K_{nm} in eq. (7) as element of an $N * M$ data kernel matrix $\underline{\underline{K}}$ and the solution coefficient h_{kn} in eq. (8) as element of an $M * N$ solution matrix $\underline{\underline{H}}$, which represent the so-called pseudo-inverse of matrix $\underline{\underline{K}}$. Inserting y_n from eq. (6) into eq. (7) and combining then this equation with eq. (8) shows that the resolution coefficients are elements of an $M * M$ resolution matrix $\underline{\underline{A}} = \underline{\underline{H}}\,\underline{\underline{K}}$.

We distinguish now between two models on the basis of *global* solution criteria, which involve either *all* data or *all* model parameters, and two models on the basis of *local* solution criteria in reference to the mean model at a specified target layer or grid cell. Standard models of the first kind are least squares models with

$$\underline{\underline{H}} = (\underline{\underline{K}}^T \underline{\underline{K}})^{-1} \underline{\underline{K}}^T \, , \tag{10}$$

which minimise the sum of all squared misfit residuals δy_n^2 , and minimum norm models with

$$\underline{\underline{H}} = \underline{\underline{K}}^T (\underline{\underline{K}}\,\underline{\underline{K}}^T)^{-1} \tag{11}$$

which minimise the sum of all squared model parameters x_m^2 under the side condition that the model accounts for the data with zero misfit residuals. As a rule, either model may explain the data too well, in case of the minimum norm model that is obviously always so for error-bearing data. In addition the matrices $\underline{\underline{K}}^T \underline{\underline{K}}$ and $\underline{\underline{K}}\,\underline{\underline{K}}^T$ usually are ill-conditioned for inversion. Therefore a stabilised pseudo-inverse of matrix $\underline{\underline{K}}$ is in common use according to

$$\underline{\underline{H}} = (\underline{\underline{K}}^T \underline{\underline{K}} + \alpha^2)^{-1} \underline{\underline{K}}^T = \underline{\underline{K}}^T (\underline{\underline{K}}\,\underline{\underline{K}}^T + \alpha^2)^{-1} . \tag{12}$$

Interpretations on its basis lead to “regularized” models, which neither yield the best possible fir to the data nor do they provide the smoothed possible model with zero misfit residuals. This trade-off between model fit and model smoothness is controlled by Tikhonov’s regularisation parameter α^2. See Protokoll EMTF Kolloquium Wohldenberg”, p. 88-89, (2005), how to conduct an efficient search for an appropriate value of α^2, providing equality of δy and Δy from eqs (1) and (2) for an interpretation within error limits.

Models based on local criteria minimise either the resolution measures Δ_k of eqs (5) or the squared model error $\Delta\bar{x}_k^2$ according to eq. (9). Since in the first case model errors become unacceptably large and in the second case the same applies to the poorness of the resolution, the minimum of a linear combination of Δ_k and $\Delta\bar{x}_k^2$ leads to the here indispensable trade-off between model resolution and model accuracy. There are no established rules how to conduct

this Backus-Gilbert second trade-off. In the above cited reference it is suggested to adjust the trade-off that the regularized model has the same error for the respective target layer or cell.

4. 1D interpretations

The foregoing sections have presented the basic ideas behind our treatment of the non-linear inverse problem. We turn now to their implementation when interpreting data of increasing complexity. As in the first two sections we return to spatially continuous models, but it is clear that in practical applications, as they will follow in Section 7, the models will be subdivided again into uniform domains and represented by sets of discrete model parameters.

Starting with 1D model, they are derived from the surface response at a single site, i.e. from the impedance $Z(\omega_n)$ for a quasi-uniform inducing field. The functional F_n will be the Ψ-algorithm. See the Protokoll EMTF Kolloquium Wohldenberg, p. 85-87, (2005) for a description of this algorithm. Its key property is that it allows a straightforward decomposition of the integrand of the basic integral equation into a to second order model-independent data kernel, connecting the logarithm of the impedance with the logarithm of resistivity. Hence, the 1D version eq. (3) is

$$y_n = \int_0^\infty K_n(x \mid 0, z') \cdot x(z')\, dz' + \delta y_n \qquad (13).$$

with

$$y_n = \ln\{Z(\omega_n)/Z_0(\omega_n)\} = \ln\{\rho_a(\omega_n)/\rho_0\} + 2i[\pi/4 - \varphi(\omega_n)]\ , \qquad (13a)$$

as datum,

$$x(z') = \ln\{\rho(z')/\rho_0\} \qquad (13b)$$

as model parameter and

$$K_n^{(0)}(0, z') = 2\alpha_n \exp\{2\alpha_n z'\} \qquad (13c)$$

as model-independent approximated data kernel, where $\alpha_n = \sqrt{\mu_0 \omega_n / \rho_0}$; ρ_0 is an arbitrary scaling resistivity and $Z_0(\omega_n) = \sqrt{i\omega_n \rho_0 / \mu_0}$ the surface impedance of a uniform half-space of resistivity ρ_0, while $\rho_a = \mu_0 / \omega_n \cdot |Z(\omega_n)|^2$ and $\varphi = \arg\{Z(\omega_n)\}$ are apparent resistivity and phase in their usual definitions.

The depth z' is not the real depth z, however, but a conductivity-weighted depth

$$z'(z) = \int_0^z \sqrt{\rho_0 / \rho(\hat{z})}\, d\hat{z}\ . \qquad (14)$$

This transformation of $\rho(z)$ into $\rho(z')$ expands low resistivity sections with $\rho(z) < \rho_0$ and thus strong attenuation of the downward diffusing EM field, while it compresses high resistivity sections with $\rho(z) > \rho_0$ and small attenuation, thus balancing the overall rate of downward attenuation. When in practice a layered model concept is used, with d_m denoting

the thickness of the *m-th* layer in real depth, then eq. (14) implies that $d_m / \sqrt{\rho_m} = d_0 / \sqrt{\rho_0}$ is the same for all layers, when $\rho(z')$ is equally subdivide into constant depth increments d_0 above a concluding uniform half-space. Once the layer resistivities have been determined, the model in true depth is readily reconstructed from $d_m = d_0 \sqrt{\rho_m / \rho_0}$, noting that in this way layer thicknesses are not part of the interpretation. For a quasi-continuous model with many layers, the specific choice of d_0 is practically without influence, since any resistivity distribution can be approximated with a sufficiently finely subdivided model. If the model consists, however, only of a few layers to keep the solution with $M << N$ closely to a least squares solution, then the choice of d_0 matters and it should be optimized to obtain the best possible fit. Under certain circumstances it may be useful to relax the stringent relation from above between thickness and resistivity by introducing layer weights w_m in $d_m = w_m d_0 \sqrt{\rho_m / \rho_0}$. They can be preset to place boundaries at the depth of seismic discontinuities, for example, or they are derived in a separate least squares analysis for a sequence of sedimentary strata of more or less known resistivity.

The 1D version of eq. (5b) is

$$\Delta(z'_k) = \int_0^\infty a(z'_k, z')^2 \, J_0 \cdot (z' - z'_k)^2 \, dz' \tag{15}$$

with $J_0 = 12$, and the resulting Backus-Gilbert spread can be regarded as the half-width of the resolution kernel on a z' depth scale. In general it is sufficient to assess the resolution of 1D models with the uses of the approximated data kernel of eq. (13c), that is without reference to a specific model.. Furthermore, the integrals involved in the minimisation of the spread can be solved then in closed form. It has been found that their numerical integration with the use of mode-dependent data kernels leads more or less to the same results. See Protokoll EMFT Kolloquium Wohldenberg (2006) for demonstrations.

5. 2D interpretations in E-polarisation

The modelling space *A* will be the cross-section of a 2D structure in the *(y,z)* plane, striking in x-direction.. We assume induction by a quasi-uniform field with a linearly polarized electric vector in strike direction, and the data to be interpreted are the magneto-telluric impedances and the transfer functions of geomagnetic depth sounding (GDS), which have been derived from observations in a chain of field sites across the 2D structure. It is imbedded into a normal structure of conductivity $\sigma_n(z')$ which we presume to be known from 1D interpretations of the impedance $Z_n = E_{nx} / B_{ny}$ at a safe distance. To be found is $\sigma_a(y', z') = \sigma(y', z') - \sigma_n(z')$ within *A* from the anomalous parts of the observed surface field in terms of their transfer functions. Omitting their non-existing dependencies on *x* and observing that for quasi-uniform fields B_{nz} is zero, these field components are

$$E_{ax}(y,0) = E_x / y,0) - E_{nz}(0) = [Z_{xy}(y) - Z_n] \cdot B_{ny}(0) \tag{16}$$

with Z_{xy} as E-polarisation impedance tensor element, and

$$B_{ay}(y,0) = B_y(y,0) - B_{ny}(0) = d_D(y) \cdot B_{ny}(0)\,, \qquad B_{az}(y,0) = z_D(y) \cdot B_{ny}(0) \tag{17}$$

with d_D and z_D as GDS transfer functions. Note that it is necessary in this context to relate the electric field as well as the two magnetic field components to the *normal* part of the horizontal magnetic surface field B_{ny} as it would have been observed in the hypothetical absence of the 2D structure and which can be inferred from observations at a great distance..

For the derivation of the integral equation to interpret these data, we start from the 2D forward problem in E-polarisation. With $\underline{r} = (y,z)$ and $\underline{r}' = (y',z')$ dependencies on x are omitted again, also dependencies on frequency are not expressed explicitly. Then according to the integral method the internal electric field follows for a given model and frequency from

$$E_{ax}(\underline{r}) = -i\omega_n\mu_0 \int_A G^{(TE)}(\sigma_n \mid \underline{r},\underline{r}')\, E_x(\underline{r}')\, \sigma_a(\underline{r}')\, d\underline{r}'\,, \tag{18}$$

where $E_{nx}(z')$ within the normal structure is assumed to be known and with $G^{(TE)}$ as Green's function for E-polarisation. It connects an oscillating electric line current in x-direction, passing through $\underline{r}'$, with the electric field which it generates in the same direction at $\underline{r}$. The sole dependence of $G^{(TE)}$ on the normal structure is indicated with σ_n among its arguments. Cf. Aarhus Lecture Notes, p.42 (1975). Since this structure is known, we presume the same for Green's function. Details about their derivation can also be found in the cited reference and in Vorlesungs-Skript 1992/93, Blatt 17-20.

We assume that $E_x(\underline{r}')$ within A has been determined, either by solving eq. (18) or by another method of forward modelling. Then the 2D version of eq. (3) to interpret E_{ay} as datum follows from eq. (18) readily as

$$E_{ax}(y,0) = -i\omega_n\mu_0 \int_A G^{(TE)}(\sigma_n \mid y,0;\underline{r}')\, E_x(\underline{r}')\, \sigma_a(\underline{r}')\, d\underline{r}' + \delta E_{ax}(y,0)\,. \tag{19a}$$

For a corresponding derivation of integral equations for the anomalous magnetic field as datum, we note that according to Faraday's law $B_{ay} = -i\omega_n\, \partial E_{ax}/\partial z$ and $B_{az} = +i\omega_n\, \partial E_{ax}/\partial y$ when $E_{ay} = E_{az} = 0$, and that in the integrand of eq. (18) only Green's function depends on the field point coordinates. Denoting with subscripts their respective derivative for $z = 0$, these equations follow in the same way from eq.(18) as

$$B_{ay}(y,0) = \quad +\mu_0 \int_A G_z^{(TE)}(\sigma_n \mid y,0;\underline{r}')\, E_x(\underline{r}')\, \sigma_a(\underline{r}')\, d\underline{r}' + \delta B_{ay}(y,0)\,, \tag{19b}$$

$$B_{az}(y,0) = \quad -\mu_0 \int_A G_y^{(TE)}(\sigma_n \mid y,0;\underline{r}')\, E_x(\underline{r}')\, \sigma_a(\underline{r}')\, d\underline{r}' + \delta B_{az}(y,0)\,. \tag{19c}$$

Evidently the anomalous part of the conductivity, preferably in the dimensionless form

$$S(\underline{r}') = \sigma_a(\underline{r}')/\sigma_n(z')\,, \tag{20}$$

is a natural choice for a model parameter, which identifies the product of Green's function times $\sigma_n(z')$ with the internal electric field E_x as data kernel. The latter consists of a known normal part $E_{nx}(z')$ and an initially unknown anomalous part $E_{ax}(y',z')$, which when ignored defines the model-independent data kernel for the derivation of the starting model. The iterative evaluation of eqs (19) follows then the same general path as outlined in Section 2. There are three data sets to choose from, which can be used either alone or in combination.

The 2D version of eq. (5b) is

$$\Delta(\underline{r}'_k) = \int_A a\ (\underline{r}'_k, \underline{r}')^2\, J_0 \cdot (y' - y'_k)^2 \cdot (z' - z'_k)^2\, d\underline{r}', \tag{21}$$

yielding an areal measure of resolution. A circle with radius $\sqrt{\Delta(\underline{r}'_k)/\pi}$, drawn around the target point, visualizes the cross-section, over which the respective model parameter represents an average.

6. 2D interpretations in B-polarisation

The set-up of the model and field sites is the same as in the previous section, except that now the *magnetic* vector of the quasi-uniform inducing field is in strike direction. Since the magnetic surface field is without anomalous part and thereby without information about internal conditions, the sole field component available for interpretation is the horizontal component E_y of the .electric surface field. In principle also its vertical component just below the surface could be used. It is not easily accessible to observations, however. We presume again that the normal conductivity structure with the 1D impedance $Z_n = -E_{ny}/B_{nx}$ is known and thus base the interpretation on the anomalous part of E_y given by

$$E_{ay}(y,0) = E_y(y,0) - E_{ny}(0) = [Z_{yx}(y) + Z_n] \cdot B_{nx}(0) \tag{22}$$

with Z_{yx} as impedance tensor element for B-polarisation.

The simple boundary condition for the magnetic field conceals the forthcoming difficulties, which we shall face when deriving the integral equation for E_{ay}. They arise from the presence of up and down going currents within and around the anomalous cross-section, also from the presence of electric charges where the conductivity changes gradually or abruptly. Therefore the integral method is rarely used for solving the forward problem in B-polarisation, with such notable exemptions as Fluche's thesis (1992). In the integral B_x takes the place of E_x and resistivity ρ the place of conductivity σ.

Let in analogy to eq. (20)

$$R(\underline{r}') = \rho_a(\underline{r}')/\rho_n(z') \tag{23}$$

denote a dimensionless measure for the anomalous part of resistivity at the internal point $\underline{r}'$ and $R(\underline{r})$ the same for the field point $\underline{r}$. Then the integral equation for deriving $B_x(\underline{r}')$ for a known normal part $B_{nx}(z')$ and model is

$$[1+R(\underline{r})]\cdot B_{ax}(\underline{r})+R(\underline{r})\cdot B_{nx}(z)=\int_A \{i\omega_n\mu_0\, G^{(TM)}(\rho_n\mid \underline{r},\underline{r}')\cdot R(\underline{r}')$$

$$+\rho_n(z')[grad\,R\cdot grad\,G^{(TM)}]\}\cdot B_x(\underline{r}')\,d\underline{r}' \quad . \tag{24}$$

Cf. Aarhus Lecture Notes, p 46-47 (1975). The complications against the corresponding equation in the case of E-polarisation are obvious. On the left appears in addition to the anomalous part B_{ax} also its normal part. The first part of the integrand on the right resembles the integrand in eq. (18) for E-polarisation except that Green's function for B-polarisation has to be used. Its connects a chain of oscillating magnetic dipoles in x-direction, passing through the internal point $\underline{r}'$, with the magnetic TM field it generates in the same direction at the field point $\underline{r}$. Green's function depends again solely on the known normal resistivity structure, as indicated, and we presume again that it has been derived beforehand for the involved set of points. Details about their actual determination can be found in the cited references in connection with eq. (18). Further complications arise when integrating over the second part. For a modelling cross-section subdivided into uniform grid cells this integration takes the form of integrals along cell boundaries and thereby accounts for accumulated charges on them. See the Appendix for details.

Also the connection between the magnetic field and the electric field is not as straightforward as for E-polarisation. The now relevant Ampere's law connects the spatial derivatives of the magnetic field with the current density $j_y = j_{ny} + j_{ay} = E_y/\rho$ rather than with the electric field itself. For $B_z = 0$ this law implies that $\partial B_{nx}/\partial z = \mu_0 j_{ny}$ and $\partial B_{ax}/\partial z = \mu_o j_{ay}$, yielding

$$\mu_0 E_{ay} = \rho\,\partial B_{ax}/\partial z + \rho_a\,\partial B_{nx}/\partial z\,. \tag{25}$$

We multiply now eq. (24) on both sides with $\rho_n(z=+0)$ and differentiate both side with respect to z at z=+0 just below the surface, assuming that $\partial R/\partial z \to 0$ for $z \to +0$, i.e. that the topmost model is uniform in vertical direction. The result is

$$\rho_n(+0)\cdot\frac{\partial}{\partial z}\int_A ....d\underline{r}' = \rho(y,+0)\frac{\partial B_{ax}}{\partial z}\mid_{z=+0} + \rho_a(y,+0)\frac{\partial B_{nx}}{\partial z}\mid_{z=+0}\ .$$

Equating the expression on the right, divided by μ_0, with $j_{ay}(y,0)$ from eq. (25) leads in combination with eq. (24) for $z=+0$ to the integral equation for E_{ay} as datum. Thus the 2D version of eq. (3) for B-polarisation is

$$E_{ay}(y,0) = \rho_n(+0)/\mu_0 \cdot \int_A \{i\omega_n\mu_0\, G_z^{(TM)}(\rho_n\mid y,+0;\underline{r}')\cdot R(\underline{r}')$$

$$+\rho_n(z')[grad\,R\cdot grad\,G_z^{(TM)}]\}\cdot B_x(\underline{r}')\,d\underline{r}' + \delta E_{ay}(y,0)\,. \tag{26}$$

The subscript to Green's function implies again differentiation with respect to z at $z = +0$. In the numerical solution of eq. (26) further problems arise from the involvement of second derivatives of Green's function in $grad\,(\partial G_z^{(TM)} / \partial z)$. They are overcome by integrations with Green's function split into "transient" and "quasi-static" parts, as outlined in the Appendix.

The integral corresponds in its first part to eq. (19b) for B_{ay} as datum, thereby suggesting in analogy R as the appropriate model parameter for B-polarisation. This choice defines for the first part the product of Green's function and B_x as data kernel. It will be a special topic of the Appendix to show that also the second part of the integrand can be decomposed into a data kernel, involving the integrals along boundaries, and the same model parameter $R(\underline{r}')$. In either case, the iterative process to solve eq. (26) towards this parameter will be initiated by replacing $B_x(\underline{r}')$ with its normal value $B_{nx}(z')$ for the derivation of a starting model. The definition of an areal measure of resolution will be the same as for E-polarisation in eq. (21).

Concluding herewith the sections on 2D interpretation, we note that the suggested different choices of model parameters for E- and B-polarisation exclude a joint inversion of both polarisations, at least within the framework of the here adopted method of interpretation. Only in the case of very moderate anomalies this may be possible We infer from eqs (20) and (23) that $(1+S)\cdot(1+R) = 1$ or $R = -S/(1+S)$. Thus, when S is small against unity for $\sigma_a << \sigma_n$, we can replace R in eq. (26) by $-S$ and facilitate thereby a joint inversion. But in general it seems that the specific information contents of 2D observations will be more fully exploited by deriving *conductivity models* from E-polarisation data and *resistivity models* from B-polarisation data. This distinction reflects the increased sensitivity of E-polarisation to interspersed good conductors due to the horizontal flow of induced currents, while vertical currents associated with B-polarisation account for their superior response to interspersed resistors.

7. 3D interpretations – an outlook

We assume that observations have been carried out in a network of field sites, and that for each site and a given polarisation MT impedances have been obtained for the two components of the electric field and GDS transfer functions for the three components of the anomalous magnetic field. The electric vector of a quasi-uniform inducing field shall be either in x-direction or in y-direction, and in this way we shall distinguish between transfer functions for *x- polarisation* and *y-polarisation*. The datum for interpretation can be anyone of these ten transfer functions, either alone within the network of sites or in combination with others.

As before far-away observation are assumed to have established the conductivity for the normal structure, into which the 3D modelling space is embedded, yielding $Z_n = E_{nx} / B_{ny}$ as known 1D impedance for x-polarisation and $Z_n = -E_{ny} / B_{nx}$ as the same impedance for y-polarisation. Hence, with $\sigma_n(z')$ being known, the interpretation will be based on the anomalous parts of the electric and magnetic surface fields to determine $\sigma_a(\underline{r}')$. In terms of their transfer functions the anomalous field components to be interpreted are

$$E_{ax} = E_x - E_{nx} = (Z_{xy} - Z_n)\cdot B_{ny} \qquad E_{ay} = E_y = Z_{yy}\cdot B_{ny} \qquad (27a)$$

$$B_{ax} = B_x = h_D \cdot B_{ny}, \qquad B_{ay} = B_y - B_{ny} = d_D \cdot B_{ny}, \qquad B_{az} = B_z = z_D \cdot B_{ny}$$

for x-polarisation and

$$E_{ax} = E_x = Z_{xx} \cdot B_{nx}\,, \qquad E_{ay} = E_y - E_{ny} = (Z_{yx} + Z_n) \cdot B_{nx}\,, \tag{27b}$$
$$B_{ax} = B_x - B_{nx} = h_H \cdot B_{nx}\,, \qquad B_{ay} = B_y = d_H \cdot B_{nx}\,, \qquad B_{az} = B_{zz} = z_H \cdot B_{nx}$$

for y-polarisation, noting that for quasi-uniform inducing fields $B_{nz} = 0$. It should be observed that once more all transfer functions are in reference to the *normal* horizontal magnetic field as it may have been observed at a great distance from the anomaly. This is an absolute requirement for the here proposed approach of interpretation. If for one reason or the other some nearby field site is chosen as a substitute, it is necessary to re-calculate the transfer functions repeatedly within the iterative process, using for their transformation the modelled GDS transfer functions of the reference site for B_{ax} and B_{ay}.

For objective reasons the 3D forward problem is commonly formulated in terms of the electric field. Within the framework of the integral method the extension from 2D and E-polarisation to 3D implies that Green vectors

$$\underline{G}_i = G_{i1}\,\underline{\hat{x}} + G_{i2}\,\underline{\hat{y}} + G_{i3}\,\underline{\hat{z}} \qquad (i, j = 1,2,3 \text{ for } x, y, z)$$

take the place of Green's function, field vectors $\underline{E}(z')$ the place of E_x and the scalar product of these two vectors the place of the product of Green's functi0on with E_x. These modifications convert eq. (18) into

$$E_{a\,i}(\underline{r}) = -i\omega\mu_0 \int_A [\underline{G}_i\,(\sigma_n\,|\underline{r}, \underline{r}') \cdot \underline{E}(\underline{r}')\,]\sigma_a(\underline{r}')\,d\underline{r}' \tag{28}$$

as basic equation for 3D modelling, from which follow then the integral equations to interpret the various MT and GDS data. Cf. Aarhus Lecture Notes, p. 50 (1975). The components G_{ij} of the Green vector relate the electric field in i-direction at the field point $\underline{r}$ to the causing electric dipole in j-direction at the internal point $\underline{r}'$. Since these components are determined again solely by the surrounding normal structure, we assume them to be known.

Starting then with E_{ax} at the Earth's surface, we obtain from eq, (28) as the 3D version of eq. (3) for this datum

$$E_{ax}(x, y, 0) = -i\omega\mu_0 \int_A [\underline{G}_x\,(\sigma_n \mid x, y, 0\,; \underline{r}') \cdot \underline{E}(\underline{r}')]\,\sigma_a(\underline{r}')\,d\underline{r}' + \delta E_{ax}(x, y, 0) \tag{29}$$

with a corresponding integral equation for E_{ay}. Thus the data kernel for σ_a as model parameter is given by the scalar product of Green vectors $\underline{G}_x$ or $\underline{G}_y$ with the internal electric field vector.

Turning now to the integral equations for the components of the anomalous magnetic field, Faraday's law implies that with $\partial E_{az} / \partial x = \partial E_{az} / \partial y = 0$ just below the Earth's surface

$$B_{ax} = \frac{1}{i\omega}\frac{\partial E_{ay}}{\partial z} \;\; , \; B_{ay} = -\frac{1}{i\omega}\frac{\partial E_{ax}}{\partial z} , \;\; B_{az} = \frac{1}{i\omega}\left(\frac{\partial E_{ax}}{\partial y} - \frac{\partial E_{ay}}{\partial x}\right) \;\; .$$

Differentiating eq. (28) with respect to the field point coordinates affects again only the components of the Green vectors. Denoting with the added subscript their respective differentiation at $z = 0$, the integral equations for the three anomalous magnetic field components are

$$B_{ax}(x,y,0) = -\mu_0 \int_A [\underline{G}_{yz}(\sigma_n \mid x,y,0\,;\underline{r}') \cdot \underline{E}(\underline{r}')]\, \sigma_a(\underline{r}')\, d\underline{r}' + \delta B_{ax}(x,y,0) \;\; , \qquad (30a)$$

$$B_{ay}(x,y,0) = +\mu_0 \int_A [\underline{G}_{xz}(\sigma_n \mid x,y,0\,;\underline{r}') \cdot \underline{E}(\underline{r}')]\, \sigma_a(\underline{r}')\, d\underline{r}' + \delta B_{ay}(x,y,0) , \qquad (30b)$$

$$B_{az}(x,y,0) = -\mu_0 \int_A [\{\underline{G}_{xy}(\sigma_n \mid x,y,0\,;\underline{r}') - \underline{G}_{yx}(\sigma_n \mid x,y,0\,;\underline{r}')\} \cdot \underline{E}(\underline{r}')]\, \sigma_a(\underline{r}')\, d\underline{r}' + \delta B_{az}(x,y,0) \;\; . \qquad (30c)$$

Depending on the polarisation, the components of the internal electric field vectors, as they appear in eqs (29 and (30), are

$$E_x(\underline{r}') = E_{nx}(z') + E_{ax}(\underline{r}') \;\; , \qquad E_y(\underline{r}') = E_{ay}(\underline{r}') \;\; , \qquad E_z(\underline{r}') = E_{az}(\underline{r}') \qquad (31a)$$

for x-polarisation and

$$E_x(\underline{r}') = E_{ax}(\underline{r}') \;\; , \qquad E_y(\underline{r}') = E_{ny}(z') + E_{ay}(\underline{r}') \;\; , \qquad E_z(\underline{r}') = E_{az}(\underline{r}') \qquad (31b)$$

for y-polarisation. Their anomalous parts, which are initially unknown, are omitted when defining the model-independent data kernel to start iterations according to Section 2. A 3D volume measure of resolution follows from eq. (21) after adding $(x - x')^2$ as factor to the integrand.

So far 3D interpretations appear as a straightforward extension of 2D interpretations for E-polarisation. But there exists a certain bias with regard to the resulting models. In 2D and E-polarisation MT as well as GDS data belong to anomalous fields in the same TE mode and, as pointed out in the previous section, they will be particularly responsive to conducting regions in the Earth. MT data in B-polarisation belong to an anomalous electric field which is exclusively in the TM mode. Their anomalous part is therefore more sensitive to resistive regions. In 3D, however, only GDS data represent surface fields in the TE mode and thus maintain their sensitivity to conductors, while MT data are related now to anomalous electric surface fields in both TE and TM modes. Consequently in their anomalous parts they should be less responsive to conducting regions than GDS data, but more responsive to resistive regions. Thus, the question arises, whether MT data in their anomalous parts can be split according to modes and then interpreted separately with either conductivity or resistivity models as in 2D.

In concluding this section on 3D interpretations we explore ways and means to achieve the just stated separation. There are two options to do so. Firstly, the vertical electric field just above the Earth's surface belongs exclusively to a TM-mode field in the air space It is difficult to observe, however, but this may not be necessary. In a closely spaced network of

field sites it should be possible to determine with sufficient accuracy the spatial derivatives of the horizontal electric components $\partial E_x / \partial x$ and $\partial E_y / \partial y$. Taking their sum eliminates their TE-mode portions and, because the remaining TM-mode portion belongs to a potential field,

$$\partial E_x / \partial x + \partial E_y / \partial y = -\partial E_z / \partial z \,|_{z=-0} \,. \tag{32}$$

This expression will be particularly responsive to internal charge accumulations. Cf. Extended Abstract EM Induction Workshop Hyderabad (2004).

In an alternative approach, based on Faraday's law, the vertical magnetic component within a network of sites is converted into the TE-mode portion of the anomalous electric surface field, which when subtracted from the total anomalous field yields its TM-mode portion. Cf. Becken & Pedersen (2003) for details. In order to interpret the thus isolated TM-modes with resistivity models, one has to proceed from a formulation of the forward problem in terms of the magnetic field vector, which is never done. Recalling the encountered difficulties, when implementing this approach in 2D for B-polarisation, it is not clear, whether the mounting problems in an extension to 3D would be justified by a sufficiently improved response towards resistive regions in the Earth.

8. Exemplary 2D interpretations with synthetic data in both polarisations

Since the Protokoll EMFT Kolloquium Wohldenberg (2006) contain numerous examples for 1D interpretations, this final section focuses on those in 2D. See also Schmucker (1993). First a short discourse is inserted to demonstrate that the occurrence of negative model conductivities or resistivities is not necessarily restricted to extraordinary situations. The model parameter $S = \sigma_a / \sigma_n = \varpi / \sigma_n - 1$ for E-polarisation or $R = \rho_a / \rho_n = \rho / \rho_n - 1$ for B-polarisation obviously has a common lower limit of -1 for non-negative conductivities or resistivities.

Consider then a 2D model with two resistivities, $\rho_1 = 200\,\Omega m$ and $\rho_2 = 20\,\Omega m$, embedded into a 1D structure with $\rho_n = 100\,\Omega m$. With $S = \rho_n / \rho - 1$ in terms of resistivity we obtain

$$S_1 = -0.5 \;,\; S_2 = +4.0 \quad \text{and} \quad R_1 = +1.0 \;,\; R_2 = -0.8 \;.$$

If then a data-derived model parameter for E-polarisation is uncertain by more than 0.5, either because of poor data quality or poor convergence of iterations, this could push S_1 below its allowed lower limit. The Lawson-Hanson algorithm, as described in Section 1, would shift it back to $S_1 = -1$ which renders the respective parts of the model as undistinguishable from a perfect resistor. In B-polarisation even uncertainties beyond 0.2 could invoke the Lawson-Hanson algorithm to make other parts of the model to appear as perfectly conducting..

This numerical example shows that even models with moderate resistivity contrasts may be partially un-resolvable in terms of finite resistivities or conductivities. If model parameters, which are below the allowed limit, do not disappear in the course of the iterative process, the final model has "holes", where in E-polarisation the resistivity is too high to be distinguishable from a *perfect resistor* and in B-polarisation too low to be distinguishable from a *perfect conductor*.

Now the interpretation of synthetic data, comprising in the case of E-polarisation MT impedances Z_{xy} and GDS transfer functions d_D and z_D, while for B-polarisation the data set is restricted to MT impedances Z_{yx}. The modelling space is subdivided into eight grid cells of equal size with either $20\Omega m$ or $200\Omega m$. To the left and right are laterally uniform sections of $100\Omega m$ and below a uniform half-space of $10\Omega m$. This normal structure is assumed to be known and thus not part of the forthcoming interpretation. Large dots mark the position of five hypothetical field sites, for which data sets have been calculated for two frequencies as indicated, adding 5% normally distributed random errors to each datum. Skin depths vary between 17.7 km for $20\Omega m$ and 54.6 for $200\Omega m$ at 1 cpm, and they are half as big for 4 cpm, indicating that the modelling space is reasonably well exposed to an attenuated downward diffusing field.

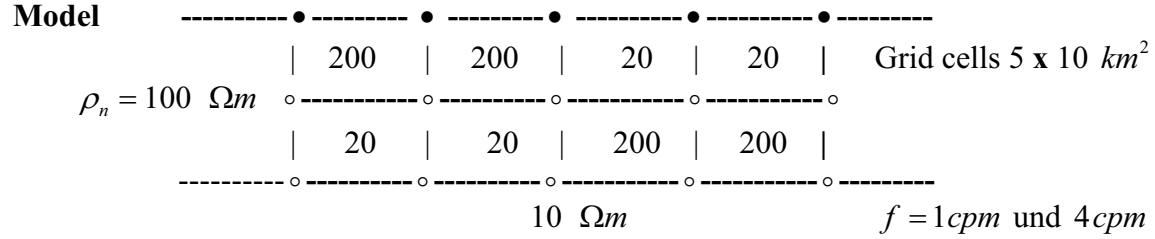

Since three field sites are positioned atop vertical boundaries, the synthetic B-polarisation data are the anomalous current densities j_{ay} just below the surface, which are continuous across these boundaries. The following modelling results are regularized least squares models, for which a regularisation parameter has been determined, which lifts the mean misfit residuals to the level of the mean data errors, so that the data are interpreted within their error limits. With complex data for five field sites and two frequencies we have $N = 20$ real data to determine $M = 8$ model parameters.

The selected model is rather complicated. In E-polarisation currents are concentrated on the left in the two bottom cells and on the right in the two top cells. B-polarisation currents which enter into the model from the left are first guided downwards to the conducting bottom section and then sharply bent upwards into the conducting top section on the right. Hence, we may expect charges of both signs to be accumulated on most boundaries, thus causing strong quasi-static contributions to the anomalous electric surface field E_{ay} as outlined in the Appendix. We may guess that the conductors in the model are well perceived by E-polarisation data, in particular on the right without overburden. But there will be problems with the resistive parts, particularly beneath a conducting overburden. B-polarisation data in contrast will be most responsive to the high resistivity sections, and it is not clear, to which extent they can recognize the conducting grid cells beneath a resistive cover on the left.

These expectations are verified by the outcome of the data interpretations as shown below. Numbers are the thereby obtained resistivities in Ωm, with modelling errors below them in parenthesis Starting with the interpretation of E-polarisation data, we note correctly determined low resistivities in the top row to the right, while they appear as slightly overestimated on the bottom on the left, possibly due to a certain bias towards the high resistivities above. As to be expected, resistivities are largely underestimated in all resistive grid cells and here also with substantial uncertainties. This applies in particular to the cells in the bottom row on the right below a shielding conducing overburden. Comparing the quality

of these modelling results from MT and GDS data, there are no large differences except that results from GDS data seem to be of slightly superior quality.

E-Polarisation

Eax

154 (160)	54 (18)	22 (4)	22 (4)
34 (8)	30 (5)	35 (7)	39 (10)

Bay

141 (38)	130 (17)	21 (1)	21 (1)
26 (1)	27 (2)	55 (14)	97 (38)

Baz

156 (19)	158 (34)	21 (1)	21 (1)
27 (2)	25 (3)	146 (109)	343 (608)

B-Polarisation

Jay

228 (27)	200 (27)	43 (16)	11 (15)
0 (-)	3 (16)	197 (12)	201 (8)

Turning to the modelling results from B-polarisation, here with j_{ay} substituting E_{ay} as datum, it is impressive to observe that the high resistivity values are all correctly determined within error limits. Evidently a conducting overburden as on the right has no shielding effect upon a resistive section beneath it, quite in contrast to E-polarisation and possibly reflecting the diagnostic effect of charged boundaries. But as anticipated their resolving power for conductors is limited, in particular when they are in greater depth. In the first cell in the bottom row on the left the resistivity is not resolvable at all, i. e. this cell appears as a perfectly conducting hole in the final model.

Even though these models have been obtained without taking model resolution and model accuracy into account, it has been found that the Backus-Gilbert trade-off between them has been optimized in the sense that the resulting models have the same model fit as the

regularized least squares models and that they interpret also the data within error limits. Furthermore, the areal resolution measure of eq. (21) corresponds closely to the chosen size of grid cells. Thus, any finer subdivision of the modelling space into, say, 32 grid cells would not have improved the resolution and any then appearing details in the models would be insignificant, when errors are taken into account.

References

Becken, M. & Pedersen, L.B., 2003. Transformation of VLF anomaly maps into apparent Resistivity and phase. *Geophysics*, **68**,497-505.

Fluche, B., 1987. Die Anwendung von Integralgleichungsmethoden auf 2D und 3D Modell-rechnungen in der erdmagnetischen Tiefensondierung. PhD Thesis Göttingen.

Kalscheuer, T. & Pedersen, L.B., 2007. A non-linear truncated SVD variance and resolution analysis of two-dimensional magnetotelluric models. Geophys. J. Int., 169,435-447.

Lawson, C.L. & Hanson, R.J., 1974. Solving least squares problems. Prentice-Hall Inc.

Schmucker, U., 1993. Erdmagnetische Tiefensondierung. Vorlesungs-Skript WS 1992/93.

Schmucker, U.,1995. 2D Modelling with Linearized Integral Equations. J. Geomag. Geoelectr., 45, 1045-1062.

Schmucker, U., 2004. Comprehensive maps of GDS and MT transfer functions. In: Extended abstracts EM Induction Workshop Hyderabad, ed. Harinarayana,T.

Schmucker, U., 2006. 1D interpretations of electromagnetic response estimates with the Psi-algorithm. In: Protokoll Kolloquium Elektromagnetische Tiefenforschung Wohldenberg, eds. Ritter, O. & Brasse. H., Deutsche Geophys. Gesellschaft, 59-90.

Schmucker, U. & Weidelt, P., 1975. Induction in the Earth. *Aarhus Lecture Notes*.

Appendix Numerical and analytical integrations of integrals along grid cell boundaries in B-polarisation

The integral in eq. (24) contains in its second part the scalar product of $grad\,R$ and $grad\,G^{(TM)}$; $R = \rho_a / \rho_n$ and differentiations are with respect to the internal point coordinates (y', z'). In order to simplify notations, we omit for Green's function references to their mode and to their dependence on σ_n, using subscripts to indicate derivatives, i. e. $G_z(\underline{r},\underline{r}')$ stands for $\partial G(\sigma_n \mid \underline{r},\underline{r}')/\partial z$. We assume that the modelling space is equally subdivided into uniform rectangular grid cells with horizontal and vertical boundaries. Then $[grad\,R \cdot grad\,G]$ reduces to $\partial R/\partial z' \cdot \partial G/\partial z'$ on horizontal and to $\partial R/\partial y' \cdot \partial G/\partial y'$ on vertical boundaries.

Let z_i denote the depth of the upper boundary of the *i-th* grid cell, which has R_i as model parameter, and let this boundary extend from $y' = y_i$ to $y' = y_i + h$, with h as width of the grid cells. We place now this boundary into a narrow strip of width 2ε and length h and

assume that R changes within the strip with depth gradually from R_{i-1} for the grid cell above to R_i. Then the contribution of this strip to the integral is given by

$$\int_{y_i}^{y_{i+h}} \int_{z_i-\varepsilon}^{z_i+\varepsilon} \rho_n(z') \frac{\partial R}{\partial z'} G_{z'}(\underline{r}; y', z') B_x(y', z') \, dz' dy' \ .$$

We observe that B_x and $\rho_n G_{z'}$ are continuous across the boundary, the latter as a measure for the vertical current. Then for $\varepsilon \to 0$

$$\int_{y_i}^{y_i+h} \int_{z_i-\varepsilon}^{z_i+\varepsilon} ..... dz' dy' = (R_i - R_{i-1}) \, \rho_n(z_i) \int_{y_i}^{y_i+h} G_{z'}(\underline{r}, y', z_i) \, B_x(y', z_i) \, dy'$$

$$\approx (R_i - R_{i-1}) \, \rho_n(z_i) \; G_{z'}(\underline{r}, y_i + h/2, z_i) \, B_x(y_i + h/2, z_i) \, h \qquad \text{(A1)}$$

with a corresponding relations for the vertical boundary involving $G_{y'}$. Their summation over all boundaries finishes the numerical integration towards the internal magnetic field.

In principle it would be possible to evaluate in the same way the second part of the integral in eq. (26) towards the anomalous electric surface field. But as to be seen a decisive portion of the integral should be solved analytically. We return to the upper boundary of the *i-th* grid cell and observe that also $\rho_n G_{zz'}$ will be continuous at horizontal boundaries. Then the contribution of this boundary to the integral is $(R_i - R_{i-1}) H_i$ in analogy to eq. (A1) with

$$H_i = \rho_n(z_i) \int_{y_i}^{y_i+h} G_{zz'}(y, 0; y', z_i) \, B_x(y', z_i) \, dy' \ . \qquad \text{(A2)}$$

Numbering the grid cells from top to bottom with $i = 1,2,.....$, their total contribution will be $R_1 \cdot H_1 + (R_2 - R_1) \cdot H_2 + (R_3 - R_2) \cdot H_3 + ……$. Re-ordering terms leads also for the second part of the integral to the decomposition into a data kernel $[(H_i - H_{i+1}) + (V_i - V_{i+1})]$ for the model parameter R_i , with V_i and V_{i+1} as integrals on the left and right vertical boundary.

Complications arise from the involvement of second derivatives of Green's function. They are overcome as follows: The products $\rho_n(z') \, G_{zz'}(y, z; y', z')$ and $\rho_n(z') \, G_{zy'}(y, z; y', z')$ are cosine and sine transforms of $\hat{G}_{zz'}(z, z')$ with $\cos(ku)$ and $\sin(ku)$ as distance factors, k as wave number and $u = y - y'$ as horizontal distance between field and internal point. The asymptotic value of $\hat{G}_{zz'}$ for $k \to \infty$ is the purely geometric attenuation factor $k \cdot \exp(-k|\, z - z'|)$. Hence, for $z = 0$ the cosine and since transforms of $[\hat{G}_{zz'} - k \cdot \exp(kz')]$ define the frequency-dependent *transient* parts of $\rho_n(z') \, G_{zz'}$ and $\rho_n(z') \, G_{zy'}$ Their remaining *static* parts as transforms of $k \cdot \exp(kz')$ are

$$\frac{1}{\pi} \frac{z_i^2 - u^2}{(z_i^2 + u^2)^2} \quad \text{for} \quad \rho_n(z_i) \; G_{zz'}(y, 0; y', z_i) \qquad \text{(A3a)}$$

on horizontal boundaries at $z' = z_{ii}$, and

$$\frac{1}{\pi}\frac{2z'v}{(z'^2+v^2)^2} \quad \text{for} \quad \rho_n(z')\, G_{z\,y'}(y,0;y_i,z') \tag{A3b}$$

on vertical boundaries at $y' = y_j$ and with $v = (y - y_j)$.

We solve integrations along boundaries numerically as in eq. (A1), when we use the transient parts of $\rho_n G_{z\,z'}$ and $\rho_n G_{z\,y'}$, but analytically with their static parts in the following approximated manner. The magnetic field within the *i-th* grid cell, including its boundaries, is expanded into a two-dimensional Taylor series. Then to first order

$$B_x(y',y') = B_x(y_0,z_0) + (y'-y_0)\cdot\frac{\partial B_x}{\partial y'} + (z'-z_0)\cdot\frac{\partial B_x}{\partial z'}$$

with (y_0, z_0) denoting the coordinates of the centre of the grid cell. For horizontal boundaries we insert the thus approximated magnetic field for $z' = z_i$ into eq. (A2), replace $\rho_n G_{z\,z'}$ by its static part from eq. (3A) and integrate the obtained purely geometric expression in closed form. The same is performed on the vertical boundary at $y' = y_i$, replacing now $\rho_n G_{z\,y'}$ by its static part from eq, (A3b). Adding the resulting contributions of all four boundaries of the *i-th* grid cell yields

$$S_i = 0\cdot B_x(y_0,z_0) + \frac{1}{\pi}\left[\log\frac{r_3}{r_1} - \log\frac{r_4}{r_2}\right]\cdot\frac{\partial B_x}{\partial y'} + \frac{1}{\pi}\left[\varphi_{34} - \varphi_{12}\right]\cdot\frac{\partial B_x}{\partial z'}\ . \tag{A4}$$

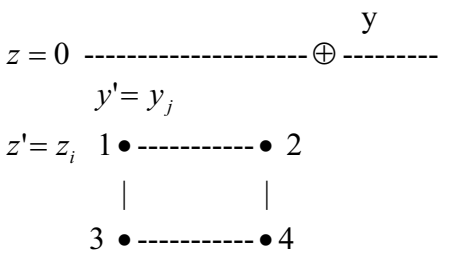

The numbers refer to the four corners of the grid cell, the angle $\varphi_{k\ell}$ implies the angle under which the boundary between the corners *k* and ℓ is seen from field point $\oplus$, and r_k is the distance between corner k and $\oplus$.

The first conclusion to be drawn from eq. (A4) is that the internal magnetic field contributes to this sum only through its spatial derivatives. Secondly, the coefficients of the magnetic field derivatives represent the potential field, which positive and negative monopoles, here electric charges, sitting on opposing boundaries generate at the field point. But since the derivatives of B_x are frequency-dependent, their contribution to E_{ay} should be named *quasi-static*, even though they arise from the static parts of $\rho_n G_{z\,z'}$ and $\rho_n G_{z\,y'}$. This applies also to characteristic so-called *static effects* for B-polarisation, among them the large "adjustment distance" from anomalies, within which E_y returns to its normal level.